Progress In Electromagnetics Research, Vol. 137, 703–725, 2013

MULTIFREQUENCY MONOPOLE ANTENNAS BY LOADING METAMATERIAL TRANSMISSION LINES WITH DUAL-SHUNT BRANCH CIRCUIT

He-Xiu Xu[1, 3, *], Guang-Ming Wang[1], Yuan-Yuan Lv[2], Mei-Qing Qi[3], Xi Gao[4], and Shuo Ge[3]

[1]Missile Institute, Air Force Engineering University, Xi'an 710051, China

[2]School of Electrics and Information Engineering, Liaoning University of Technology, Jinzhou 121000, China

[3]State Key Laboratory of Millimeter Waves, Southeast University, Nanjing 210096, China

[4]School of Information and Communications, Guilin University of Electronic Technology, Guilin 541004, China

Abstract—The theory and design of a new family of multifrequency monopole antennas by smartly loading a set of complementary metamaterial transmission line (CMTL) unit cells are investigated. The distributed CMTL elements, epsilon negative (ENG) or double negative (DNG) through incorporating additional capacitive gaps, contain a Koch-shaped extended complementary single split ring resonator pair (K-ECSSRRP) etched on the signal strip. The K-ECSSRRP features dual-shunt branches in the equivalent circuit model, rendering a distinguished resonator with dual zeroth-order resonant (ZOR) modes. By smartly controlling the element layout and loading different numbers of unit cells, ten antennas covering different communication standards (GSM1800, UMTS, Bluetooth, DMB and WIMAX) are designed and four of them are fabricated and measured. At most of operating frequencies, the antennas exhibit impedance matching better than −10 dB and normal monopolar radiation patterns. Numerical and experimental results both confirm that the single-cell or dual-cell ENG and DNG CMTL-loaded monopoles exhibit almost identical dual ZOR modes. Moreover, the loaded elements also contribute to the radiation, which is the major advantage of this

Received 24 December 2012, Accepted 21 February 2013, Scheduled 12 March 2013

* Corresponding author: He-Xiu Xu (hxxuellen@gmail.com).

prescription over previous lumped-element loadings. These antennas are compact and the multiple operating bands can be arbitrarily engineered, enabling an alternative and easy avenue toward monopoles with multifunction and high integration.

1. INTRODUCTION

Planar monopoles and dipoles [1–7] especially for the multifrequency characteristics are promising candidates in wireless portable communication system in virtue of their low profile, light weight, large service area and easy fabrication. Since artificial electromagnetic (EM) metamaterials (MTMs) [8–16] exhibit properties not commonly encountered in nature, there has been a renewed and actual interest in using the artificial EM MTMs in the design of monopole or dipole antennas [17–35] antennas, and high-gain or circularly polarized antennas [13–16, 36] over recent years. In general, the monopole or dipole antennas can be classified into three categories according to the operation mechanisms and the loading manners. The first category is based on the double negative (DNG) MTM transmission lines (TLs) or inspired from the concept of DNG MTM TLs [17–26, 32, 33] which are also termed as composite right/left handed (CRLH) TLs. These antennas can be modulated with multifrequency or broadband operation because the operating modes can be arbitrarily controlled by the well-engineered dispersion curves of the loaded TL elements. The second category is those antennas by introducing LH MTMs [27] or split ring resonators (SRRs) along the monopoles [28] and the feedlines [29] and even by embedding complementary SRRs (CSRRs) in the printed monopoles [30, 31]. In this way, the miniaturization and band-notch characteristics in an ultrawide operating band can be engineered due to the subwavelength resonance of the loaded elements. The third category is the monopole or dipole antennas built on the left handed (LH) MTM-surface made of periodically arranged LH particles [34, 35]. Through this type of loading, the antenna performances are enhanced in terms of not only the radiation behavior but also the impedance matching.

Although compact layout and multiple operation modes are achieved in aforementioned antennas made of DNG MTM TLs, the mostly reported TL elements are confined to the nonresonant-type ones by using chip elements which are not efficient radiators [17–20], [26, 33, 36] and the shunt inductors in the rarely reported distributed TLs are restricted to metallic vias which would degrade the antenna gain due to the metallic losses [21, 22]. Moreover, further miniaturization is still available and a pressing task since the

compactness is of great importance to the portable and handheld antennas. Frequency notch characteristics can be easily achieved by loading CSRRs and SRRs [28–31], however, the multiple resonances associated with multifrequency operation are limited and hardly conducted. Radiation performances may be improved by adopting the MTM surfaces [35], however, the bulk medium may complicate the design and implementation. These not well-addressed issues and insufficient strategies make an improved, alternative design that can be easily characterized and experimentally implemented a pressing task.

The focus of this paper is thus to explore a novel avenue in the implementation of fully printed monopoles with compactness as well as multifunction. Although the multifrequency strategy in the framework of dispersion engineering of artificial TLs draws some analogies with [20], the fully-printed resonant-type structures and the introduction of more operating bands on the basis of new dual-shunt branch circuit theory distinguish completely from that work by utilizing the nonresonant-type artificial TLs. The residual paper is organized as follows. In Section 2, the fundamentals and theory of the monopoles using resonant-type complementary MTM TL (CMTL) will be firstly studied. Then the CMTL elements (epsilon negative (ENG) and DNG) with dual-shunt branches are proposed by etching the Koch-shaped extended complementary single split ring resonator pair (K-ECSSRRP) [37] on the signal strip inspired from [38]. In Section 3, a new class of MTM-inspired multifrequency monopoles by smartly loading an ENG CMTL element or a DNG CMTL element in conventional microstrip-fed monopole antennas are comprehensively studied by comparing several antennas with different configurations. Two prototypes are eventually fabricated for experiment use. In Section 4, multifunctional monopoles by loading two ENG or two DNG unit cells are numerically and experimentally investigated. Section 5 concludes the whole paper. These antennas without any metallic via and lumped-element loading feature compact, low profile and completely uniplanar, rendering an easy fabrication by using simple photolithography.

2. THEORY OF THE K-ECSSRRP-LOADED MICROSTRIP-FED ENG AND DNG MONOPOLES

2.1. Fundamentals and Theoretical Background

Monopole antenna in terms of the conceptual nonresonant-type MTM TLs has been extensively studied, however, to the authors' best knowledge the distributed resonant-type artificial TL has never been reported in this discipline. The critical obstacle of pushing

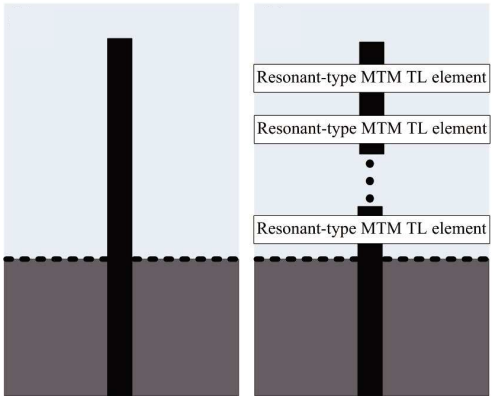

Figure 1. Sketch of the microstrip-fed monopoles. (a) Conventional monopole. (b) Conceptual monopole loaded with resonant-type MTM TL elements.

resonant-type MTM TLs in the monopole application is the structure incompatibility because the elements such as CSRRs commonly require a ground plane while the radiated part of the monopoles does not. In this paper, the resonant-type structure utilized for the monopoles is the K-ECSSRRP which was etched on ground for the harmonic suppression of a diplexer by the authors [37]. Figure 1 gives the sketch of the conventional and proposed conceptual monopoles, respectively. As can be seen, the proposed monopole is constructed by loading a class of MTM TL elements in conventional microstrip-fed counterpart. As a first step towards the monopole design, four essential parameters are defined for characterization and analysis convenience: they are the phase $\varphi_{\mathrm{MTM\,TL}}$ induced from single artificial TL element, the φ_{Mono} caused by the residual radiation part of the host monopole, the resonant modes (indices) n and the number of the utilized artificial TL element N. Similar to the monopoles by employing nonresonant-type TL elements [21], the overall possible eigenfrequencies of the monopoles by loading resonant-type elements satisfy the following resonant condition.

$$\begin{aligned} \varphi_{\mathrm{total}} &= N \times \varphi_{\mathrm{MTM\,TL}} + \varphi_{\mathrm{Mono}} = n\pi/2 \\ n &= 0, \ \pm 1, \ \pm 3, \ldots \end{aligned} \tag{1}$$

where φ_{total} is the phase shift induced across the entire antenna structure. Observation from Eq. (1) indicates that the phase induced from the host monopole and the loaded TL elements play a dominant role in determining the resonance frequency of antennas. It should be

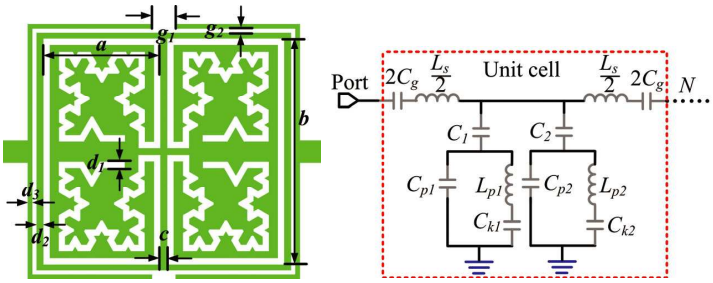

Figure 2. (a) Layout of the DNG CMTL element, and (b) corresponding equivalent circuit model of the MTM-inspired monopole loaded with N-cell DNG CMTL elements. The circuit model of the DNG element is plotted in the red dashed.

noted that stop band of the ENG or DNG TL element can also be engineered for antenna design in the case of an open circuit (infinitely large series impedance) or a resonance of the shunt branch (often referred to as the zeroth-order resonance (ZOR)) in the equivalent circuit model, which will be discussed in the upcoming section. In both cases, the current has no place to go except through the shunt branch.

2.2. CMTL Elements with Dual-shunt Branch Circuit

Figure 2 shows the layout of the DNG CMTL element and the corresponding equivalent circuit model of the MTM-inspired N-cell monopole antenna. As can be seen, the TL element consists of an inner K-ECSSRRP slot (depicted in white) etched on the square patch of a conductor strip (depicted in blue) and an outer square ring with two splits at the top and bottom position. The K-ECSSRRP evolves from the complementary single split ring resonator pair (CSSRRP) by expanding each end point of the CSSRRP with an inner smaller slot made of three second-order Koch curves and one first-order curve [37]. Although the K-ECSSRRP is etched on the signal strip, it still responses to the time-varying axial electric field and provides the electric resonant negative permittivity. The capacitive gaps between the square patch and the square ring provide the required LH capacitance C_g, rendering the magnetic resonant negative permeability. The overlapped negative permittivity and permeability enable the negative index and backward wave propagation (LH characteristic) of the DNG element.

Since the length of the capacitive gaps at both sides has been significantly extended with respect to that presented in [38], a larger C_g and thus an enhanced LH characteristic would be carried out. In the equivalent circuit model of the unit cell shown in the red dashed (similar to [37]), L_s models the inductive effect of the signal strip while the dual shunt branches model the impinging of the time-varying axial electric field to the outer CSSRRP and inner complementary Koch slot, respectively. The ENG CMTL element can be conceptually realized by removing C_g in the circuit model. This can be carried out by getting rid of the outer square ring or by filling the both splits of the ring in the physical layout. In the latter case, a hybrid resonator is shaped with a closed slot. In both cases, the dual-shunt branches maintain identical circuit elements.

Specifically, since the series gaps and the K-ECSSRRP are decoupled, the grounded fringing capacitance (C_f) of the gaps [38] should be included in the circuit model to exactly describe the behavior. However in this particular design, since the ground plane of the monopole antennas is far from the K-ECSSRRP, C_f is considerably weakened and can be neglected for analysis convenience. Moreover, C_f has nothing to do with the resonant modes of antennas but slightly affects the impedance matching in terms of reactive loading. As the dual-shunt branch circuit theory associated with LH behavior has been thoroughly studied in [39] by the authors, in this work we will concentrate on the circuit for radiated-wave design and application. Distinguished from the guided-wave design, the monopole antennas realized by the CMTL elements have an open-ended boundary. Consequently, the input impedance from input port to the output one is obtained as [40]

$$Z_{in} = -jZ_0 \cot \beta d^{\beta \to 0} = -jZ_0 \frac{1}{\beta d} = \frac{1}{Y_i}. \tag{2}$$

where Y_i in this work is the admittance of the ith shunt branch given by

$$Y_i = \frac{j\omega C_i \left[C_{pi} + C_{ki} - \omega^2 L_{pi} C_{pi} C_{ki}\right]}{C_{pi} + C_{ki} + C_i - \omega^2 L_{pi} C_{ki} (C_{pi} + C_i)}. \tag{3}$$

Therefore, the ith ZOR frequency of the CMTL element is determined by forcing Eq. (3) to be null.

$$f_{Mi} = \frac{1}{2\pi} \sqrt{\frac{C_{pi} + C_{ki}}{L_{pi} C_{ki} C_{pi}}} \tag{4}$$

Observation from Eq. (4) illustrates that f_{Mi} is determined by the dimensions of the unit cell related with the circuit parameters of the

shunt branch rather than the physical length of the entire monopole antenna.

3. MULTIFREQUENCY MONOPOLES LOADED WITH SINGLE CMTL ELEMENT

Based on the theory and analytical results, the monopoles implemented by loading an aforementioned ENG or DNG CMTL element are numerically and experimentally studied in this section. These CMTL elements can be easily integrated with the planar monopoles in which the ground plane of the radiating parts remains unaltered. The design flow starts with the conventional microstrip-fed monopole where the ground plane $L_g \times w_g$ is finely optimized to obtain a desirable impedance matching over a wide bandwidth and normal monopolar radiation with high efficiency. The length of the monopole is designed to enable the antenna to operate around GSM band (centred at 1.8 GHz). The purpose of the EM CMTL elements in the antenna design is to introduce multiple resonant modes and thus multifrequency operation. The location of the element and the length and width of the feedline ($a_2 \times w_2$) at both ends of the elements are critical factors for impedance matching over multiple bands. Through a proper design of

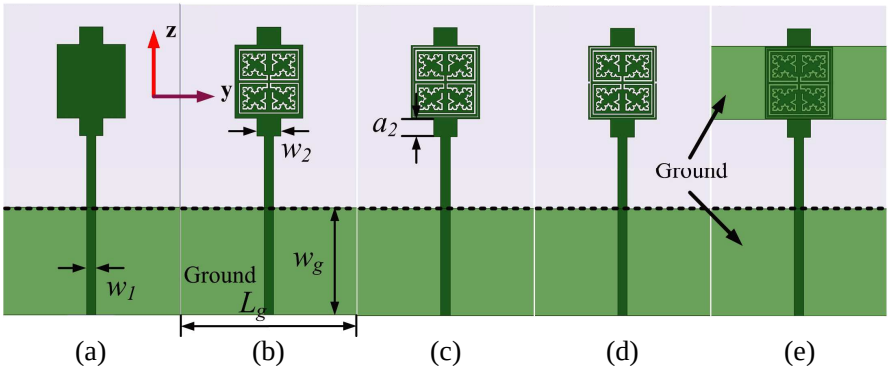

Figure 3. Layouts of the proposed single-cell K-ECSSRRP-loaded monopole antennas. (a) Conventional antenna (Case 1); (b) ENG antenna (Case 2); (c) hybrid ENG antenna (Case 3); (d) DNG antenna (Case 4); (e) hybrid ENG antenna with ground underneath the CMTL element (Case 5). The geometrical parameters of these antennas (in millimeter: mm) are $a = 5.3$, $b = 10.3$, $c = 0.3$, $g_1 = 0.4$, $g_2 = 0.2$, $d_1 = d_2 = 0.3$, $d_3 = 0.2$, $w_1 = 1.6$, $w_2 = 4$, $L_g = 30$, $w_g = 18$, and $a_2 = 1.5$.

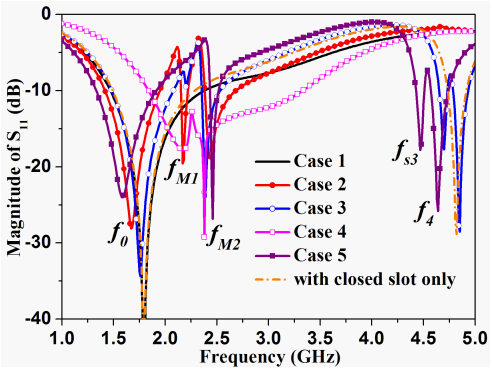

Figure 4. Comparison of simulated reflection coefficients of the proposed single-cell MTM-inspired antennas.

the CMTL elements, the antenna can be engineered to operate at the specific frequencies with arbitrary frequency ratio.

Figure 3 depicts the layouts of the proposed MTM-inspired microstrip-fed monopoles as well as the geometrical dimensions. For a comprehensive investigation, six cases are considered. They are orderly the conventional monopole without MTM loading, the monopoles by loading the ENG elements without and with (defined as hybrid ENG resonator) a closed slot, the DNG monopole, the hybrid ENG antenna with a ground plane beneath the hybrid resonator and the monopole with only the closed slot (layout not shown for brevity). In the fifth case, the ground beneath the hybrid CMTL element is not connected to the main ground of the host monopole. To this end, it acts as a ground of the hybrid CMTL element and thus facilitates an efficient radiator of the monopole rather than a feed line (if connected to the main ground). All designs and simulations are conducted in the commercial full-wave finite-element-method (FEM) EM field simulator Ansoft HFSS (Version of 13.2) and all antenna layouts with a total footprint of $1 \times 30 \times 52.6\,\text{mm}^3$ are built on the commonly available inexpensive 1mm-thick F4B substrate with dielectric constant of $\varepsilon_r = 2.2$ and loss tangent of $\tan\delta = 0.001$.

Figure 4 compares the simulated reflection coefficients of the aforementioned MTM-inspired monopoles. Following the figure, four aspects should be highlighted. 1) The CMTL loading leads to the slightly reduced operating frequency of the host monopole due to the coupling of the CMTL to the host monopole. In addition, multiple reflection dips with magnitude better than $-10\,\text{dB}$ are achieved when CMTL elements are loaded in the monopoles. 2) Of all MTM-inspired

antennas, the dual ZOR frequencies f_{M1} and f_{M2} characterized by the reflection dips are observed almost identical in all ENG and DNG cases and they are cautiously designed around the UMTS (1920–2170 MHz) and the Bluetooth (2400–2483.5 MHz) band. When a ground plane is underneath the hybrid CMTL element, see case 5, the first ZOR mode f_{M1} is weakly excited and vanishes in the resonance of the host monopole. Moreover, the monopole suffers a frequency shift downwards except for the almost constant f_{M2}. Despite these discrepancies, results between the antennas with and without ground beneath the CMTL element are in a good consistency. The enhanced

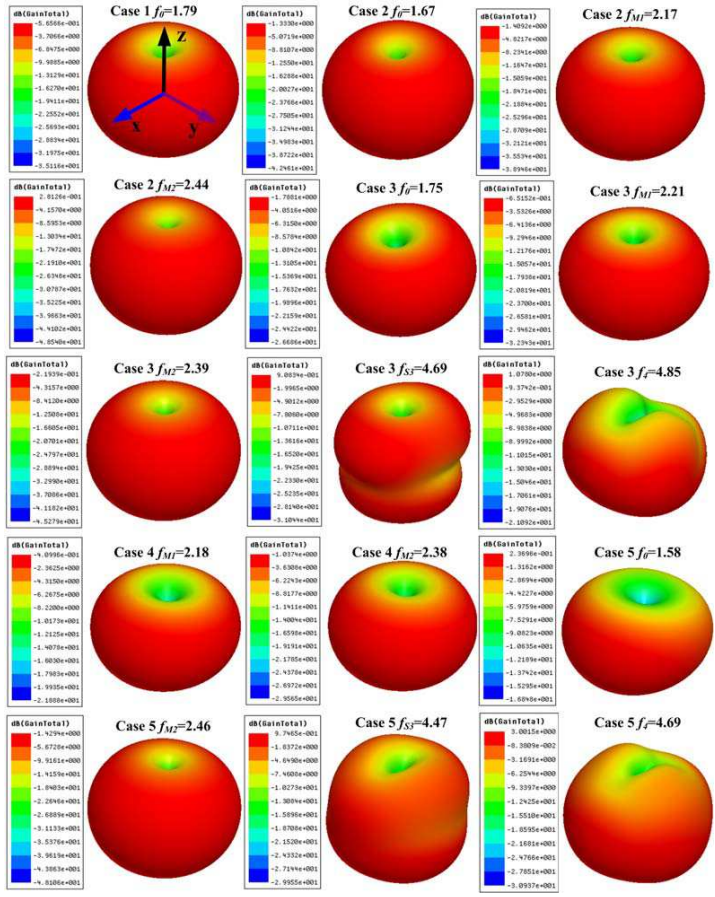

Figure 5. Simulated 3-D radiation patterns of the single-cell MTM-inspired monopoles at different resonant frequencies.

fringing capacitances C_f in virtue of the ground gives direct rise to the reduced frequency of f_0, f_{s3} and f_4 while contributes nothing to the shunt resonant tank and thus poses little effect on f_{M2}. 3) A further inspection indicates that the closed slot not only incurs an additional resonant dip around $f_{s3} = 4.5\,\text{GHz}$ but also interacts with the K-ECSSRRP, rendering the decrease of higher-order parasitic resonance f_4 after f_{s3}. This is why the higher-order resonant dip is not observed in case 2. 4) The dual ZOR resonances of the K-ECSSRRP in the DNG monopole, showing strong intensity, are in such a close proximity that they merge into a broad operation band with S_{11} better than $-10\,\text{dB}$ from 1.84 to 3.35 GHz. In this case, the host monopole integrates well with the DNG cell and it interacts with the CMTL element, facilitating a broader band around f_{M1}. Moreover, the resonant $n = +1$ mode is also excited around 3 GHz continuing on f_{M2}, rendering the broader operating band around f_{M2}. However, this is the unique feature of the DNG antenna and is impossible to be observed from any ENG antenna.

To examine the radiation characteristics, Figure 5 depicts the simulated three-dimensional (3-D) far-field patterns of the proposed ENG and DNG antennas at different operating frequencies for an intuitionistic view. As can be seen, the monopolar or quasi-monopolar radiation patterns are expected for overall operating frequencies of the proposed antennas, namely the null radiation at the broadside direction (theta = 0 and theta = pi) in *xoz*-plane while quasi-omnidirectional patterns in *xoy*-plane. The deteriorative omnidirectional pattern at f_{s3} is due to the radiation of the closed slot which also radiates and

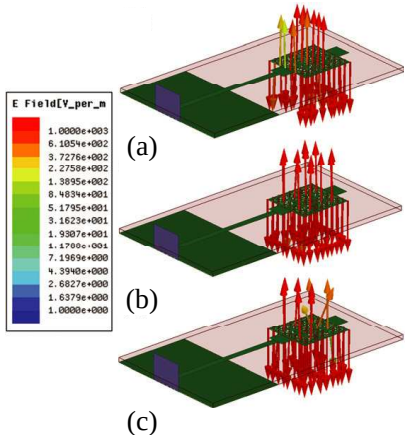

Figure 6. *E*-field distributions of the ENG MTM-inspired antenna (case 2) at f_0, f_{M1} and f_{M2}, respectively.

thus facilitates the spatial power to be re-synthesized. The degraded monopolar radiation at f_4 is natural because of the higher-order mode. A further inspection also indicates that the gain of the MTM-inspired antennas is slightly worsened on the order of 0.8 dB in comparison with conventional antenna. The negative antenna gain is due to the small ground plane which plays an important role in shaping the pattern and determining the gain. Extensive numerical results indicate that an average of 0.7 dB gain enhancement would be expected when L_g increases by 10 mm in a specific range. Nevertheless, the monopolar or quasi-monopolar radiation are always inspected, indicating that the CMTL loading helps to introduce multiple resonant modes and reduce the operating frequency of the host antenna without degrading considerably the antenna performances. This feature distinguishes the

Table 1. Comparison of performances of the proposed MTM-inspired single-cell antennas.

Antennas	Antenna gain (dB)				
	f_0	f_{M1}	f_{M2}	f_{s3}	f_4
Case 1	−0.56	-	-	-	-
Case 2	−1.33	−1.41	0.28	-	-
Case 3	−1.79	−0.65	−0.22	0.91	1.08
Case 4	-	−0.41	−1.04	-	-
Antennas	BW (GHz)				
	f_0	f_{M1}	f_{M2}	f_{s3}	f_4
Case 1	1.47–2.38	-	-	-	-
Case 2	1.41–1.95	2.15–2.22	2.38–2.69	-	-
Case 3	1.49–2.08	2.2	2.35–2.53	4.65–4.73	4.79-4.93
Case 4	-	1.84–3.34		-	-
Antennas	Radiation efficiency (%)				
	f_0	f_{M1}	f_{M2}	f_{s3}	f_4
Case 1	89.2	-	-	-	-
Case 2	93.9	69.8	94.3	-	-
Case 3	93.1	78.5	85.9	77.2	76.4
Case 4	-	97.9	72.5	-	-

Note: The bandwidth (BW) is characterized by the −10 dB reflection coefficient. For the reflection coefficients large than −10 dB the center frequency is given instead of BW. The efficiency is defined as the radiated power divided by the accepted power at the center frequency shown in Figure 5.

resulting antennas from any previous monopole and dipole made of chip elements which are usually inefficient radiators.

In fact, the CMTL element integrates well with the host monopole and also contributes to the radiation, which has been corroborated by the E-field distributions of the ENG antenna shown in Figure 6. Note that similar E-field distributions can be expected at corresponding frequencies for residual antennas. Following the figure, we learn that the x-directed E-field intensity mainly concentrates on the center of the K-ECSSRRP at f_0, whereas the uniform E-field distribution is observed in the entire outer CSSRRP and the inner complementary Koch slot at f_{M1} and f_{M2}, respectively, further confirming the dual resonances and dual-shunt branches associated with the specific localized regions. Detailed antenna performances can be referred to in Table 1. As can be concluded, the radiation efficiency slightly improves at f_0 when CMTL elements are loaded. The radiation of the K-ECSSRRP gives direct rise to the improved efficiency. This is the major advantage of our prescription for multifrequency antennas over those by loading chip components [17–20, 26, 33]. Moreover, the antenna gain and efficiency depend on the operating modes and the CMTL configuration. For instance, the gain and efficiency at f_{M2} is better than those at f_{M1} in the ENG case. By contrary, they are drastically enhanced at f_{M1} in the DNG case. The double negative permittivity and permeability around f_{M1} render the strong radiation of the CMTL element and thus give rise to this abnormal feature. The relatively low efficiency of the ENG antenna at f_{M1} with respect

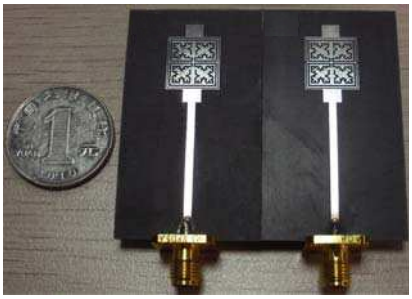

Figure 7. Fabricated prototypes of the single-cell K-ECSSRRP-loaded monopole antennas. (a) Hybrid ENG antenna. (b) DNG antenna.

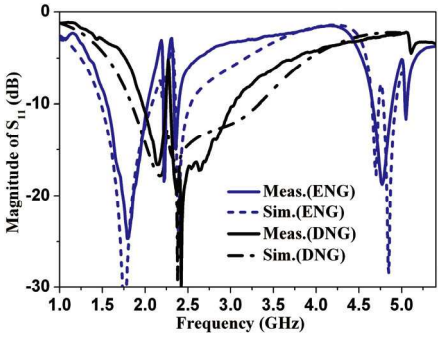

Figure 8. Simulated and measured reflection coefficients of the proposed single-cell ENG and DNG monopole antennas.

to f_0 and f_{M2} is because f_{M1} is located between two very close low efficiency dips (not shown for brevity) at which no radiation occurs, resembling the monopoles in [20]. Nevertheless, the efficiency levels with minimum value of 69.8% are very comparable relative to those presented in previous works.

For verification, the designed hybrid ENG and DNG monopoles are fabricated and measured with reflection coefficients through a N5230C vector network analyzer and the radiation patterns through a far-field measurement system in an anechoic chamber. The photograph of the fabricated prototypes is shown in Figure 7 and both prototypes are extremely compact. Figure 8 compares the simulated and the measured reflection coefficients of the both monopoles. As is observed, a desirable agreement of results between simulation and measurement is observed except for a slightly wider bandwidth at f_{s3} and small

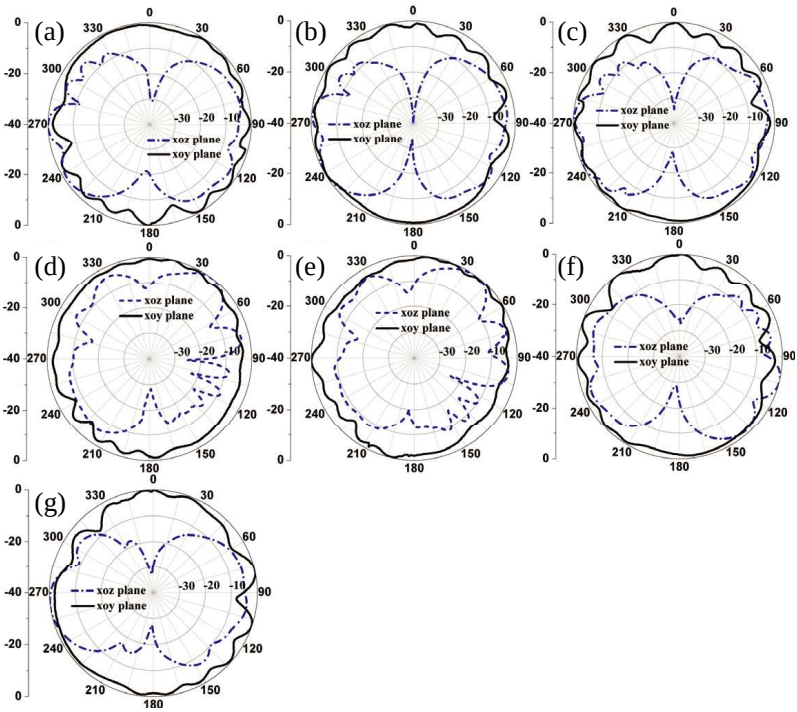

Figure 9. Measured radiation patterns of the proposed single-cell (a)–(e) hybrid ENG and (f)–(g) DNG MTM-inspired monopoles at different frequencies. (a) 1.79 GHz, (b) 2.22 GHz, (c) 2.35 GHz, (d) 4.77 GHz, (e) 5.05 GHz, (f) 2.15 GHz and (g) 2.42 GHz.

frequency shift upward at f_4 for the ENG antenna while slightly narrower bandwidth at f_{M1} and f_{M2} for the DNG antenna in the measurement. This deviation can be attributable to the small calculation error by HFSS in solving a complex structure in such a broad band and the tolerances that are inherent in the fabrication process. Over all measured bands, the reflection coefficients are better than −10 dB. Therefore, the dual ZOR modes and multifunction of the antennas have been unambiguously confirmed, indicating an efficient design. Figure 9 examines the measured co-polarized radiation patterns at different center frequencies in the *xoz*- and *xoy*-plane which correspond to two principle radiation planes. The cross-polarization levels are not the concern in this work and are not given for brevity

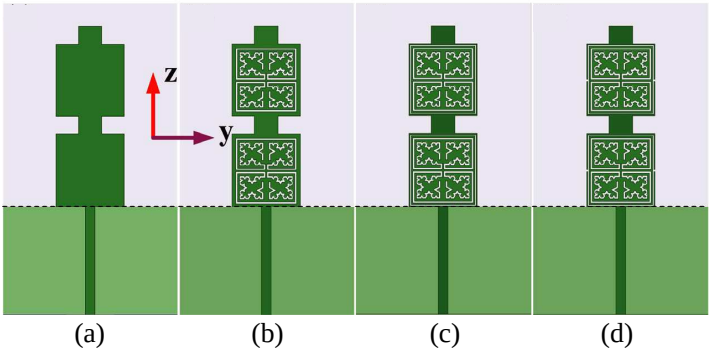

Figure 10. Layouts of the proposed dual-cell K-ECSSRRP-loaded microstrip-fed monopoles. (a) Conventional antenna (Case 1); (b) ENG antenna (Case 2); (c) hybrid ENG antenna (Case 3); (d) DNG antenna (Case 4). The geometrical parameters of these antennas are kept the same as those of single-cell MTM-inspired antennas.

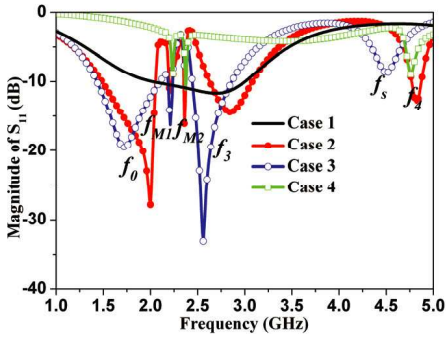

Figure 11. Comparison of simulated reflection coefficients of the proposed dual-cell monopoles.

of contents. For the sake of the clarity of figures and avoiding repetition of contents, the simulated patterns are not plotted together. As is expected at all selected frequencies, the monopolar radiations are clearly revealed from the nearly null radiation at the broadside direction in *xoz*-plane while quasi-omnidirectional patterns in *xoy*-plane.

4. MONOPOLES LOADED WITH MULTIPLE CMTL ELEMENTS

Now that the single CMTL element with different configurations has been explored for multifrequency monopoles, a natural extension is to consider the multiple CMTL elements in the monopole design and implementation. To ease the design and not lose generality, the dual-cell loading is representative and will be studied instead of by employing more elements. Figure 10 portrays the layouts

Table 2. Comparison of performances of the proposed MTM-inspired dual-cell antennas.

Antennas	Antenna gain (dB)				
	f_0	f_{M1}	f_{M2}	f_3	f_4
Case 1	−0.62	-	-	-	-
Case 2	−0.21	−1.21	−6.93	1.72	1.25
Case 3	−0.99	−1.58	−11.7	0.98	1.04
Case 4	-	−3.77	−2.84	-	1.18
Antennas	BW (GHz)				
	f_0	f_{M1}	f_{M2}	f_3	f_4
Case 1	2.03–3.01	-	-	-	-
Case 2	1.48–2.05	2.19–2.23	2.35–2.38	2.62–3.09	4.76-4.88
Case 3	1.44–2.1	2.18–2.24	2.36	2.44–2.87	4.5
Case 4	-	2.23	2.37	-	4.75
Antennas	Radiation efficiency (%)				
	f_0	f_{M1}	f_{M2}	f_3	f_4
Case 1	98.1	-	-	-	-
Case 2	94.6	75.9	13.9	98.2	75.1
Case 3	84.2	59.8	6.36	98.3	68.1
Case 4	-	66.7	60.2	-	63.4

Note: The BW and efficiency are defined as the same as Table 1 and the center frequencies are shown in Figure 12.

of the proposed dual-cell microstrip-fed monopoles with different configurations. The dual DNG elements will introduce more resonance modes according to Eq. (1) and the matching performances are expected to be worse if other geometrical parameters remain constant [20]. For characterization, the proposed antennas are also extensively analyzed in HFSS.

Figure 11 depicts the simulated reflection coefficients of the proposed dual-cell monopoles. As is expected, additional operating band centred at f_3 can be identified from the reflection dips behind f_{M2}

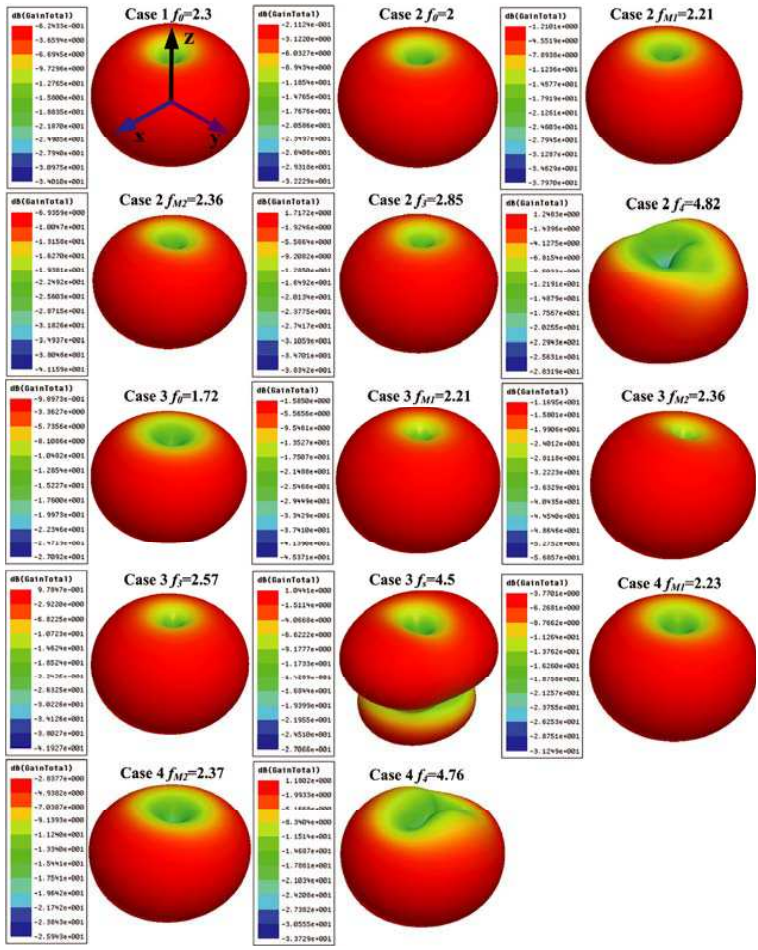

Figure 12. Simulated 3-D radiation patterns of the dual-cell MTM-inspired monopoles at different operating frequencies.

for the ENG antennas. It covers an essential Satellite Digital Mobile Broadcasting band (Satellite DMB, 2605–2655 MHz). Distinguished from the single-cell antenna, the operating band of the host monopole seems to be split into four bands (f_0, f_{M1}, f_{M2} and f_3) when two ENG CMTL elements are loaded. Despite this discrepancy, the ZOR frequencies $f_{M1} = 2.21$ and $f_{M2} = 2.36$ GHz are quantitative very similar to those 2.18 and 2.37 GHz obtained from the single-cell antenna, indicating that the ZOR modes are independent on the number of CMTL elements but dependent on the shunt-branch circuit elements associated with geometrical parameters of K-ECSSRRP. In addition, the impedance matching performances drastically degrade at f_s and f_4 while slightly worsen at the residual frequencies relative to the single-cell monopoles. This is because partial section of the host monopole is replaced by the added element. The CMTL element hardly contributes to the radiation at f_s and f_4 and thus renders a shorter monopole length and gives rise to the bad matching. However, the contribution of the CMTL elements at residual frequencies is comparable to that of the host monopole, accounting for the maintained matching performances. Note that the higher-order resonance f_4 in case 3 is observed at 5.06 GHz. The shallow reflection dip around 3.5 GHz (WiMAX band) for DNG antenna indicates a weak excitation of $n = +3$ mode and in this case the $n = +1$ mode is not excited. The monopolar radiation with peak gain on the order of 2.48 dB at 3.5 GHz further confirms the strong and efficient radiation at this frequency. Figure 12 portrays the simulated 3-D

(a) (b)

Figure 13. Fabricated prototypes of the dual-cell K-ECSSRRP-loaded monopole antennas. (a) Hybrid ENG antenna. (b) DNG antenna.

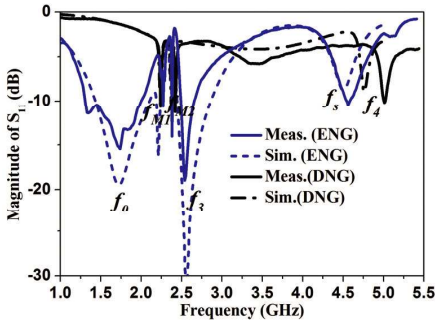

Figure 14. Comparison of the simulated and measured reflection coefficients for the dual-cell hybrid ENG and DNG monopoles.

radiation patterns at difference operating frequencies. Similar to the patterns of the monopoles loaded with single element, see Figure 5, the quasi-monopolar radiations are expected again for overall operating frequencies. The reason for the slightly deteriorative uniform patterns at f_s and f_4 is the same as that for the single-cell ENG monopoles.

Detailed performances of the four antennas are summarized in Table 2. A careful inspection of the table indicates the ENG antenna gain and efficiency suffer sharp and moderate degeneration at f_{M2} and f_{M1}, respectively and do not change considerably at the residual frequencies relative to the single-cell case. This can be successfully interpreted as the multiple cells have significantly enhanced the suppression dip and bandwidth [39], enabling the operating frequency to be very close to the low efficiency dips. This declaration finds strong

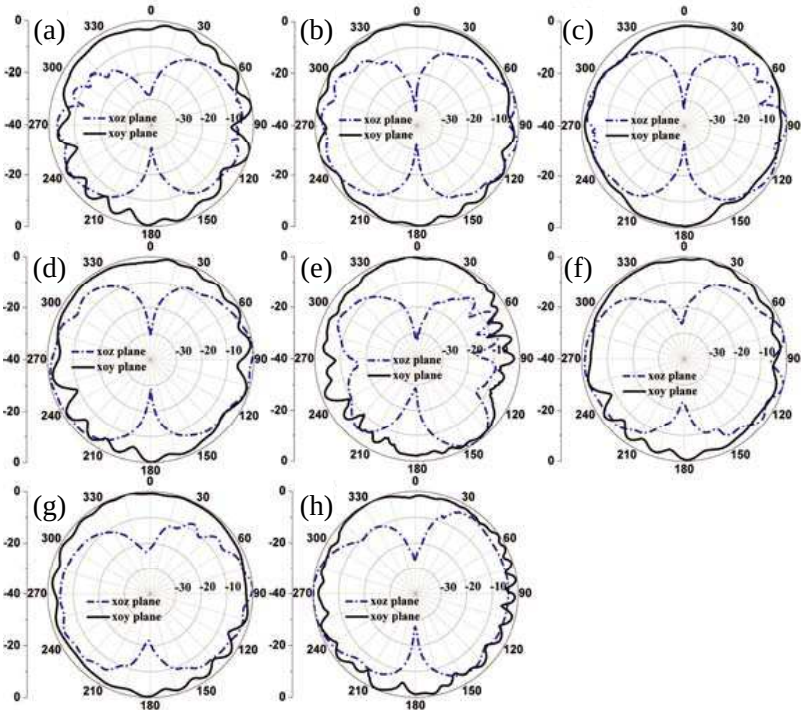

Figure 15. Measured radiation patterns of the proposed dual-cell, (a)–(e) hybrid ENG and (f)–(h) DNG MTM-inspired monopoles at different frequencies. (a) 1.8 GHz, (b) 2.27 GHz, (c) 2.38 GHz, (d) 2.54 GHz, (e) 4.57 GHz, (f) 2.24 GHz, (g) 2.42 GHz and (h) 5.01 GHz.

support from the normal gain and efficiency which benefit considerably from the double negative permittivity and permeability of the DNG antenna around f_{M2}.

For experiment use, we also fabricate the dual-cell hybrid ENG and DNG monopoles whose prototypes are given in Figure 13. The footprints of these monopoles are completely the same as those shown in Figure 7 on the same board. Figure 14 compares the simulated and the measured reflection coefficients of the both antennas. A reasonable agreement of results is achieved between the numerical calculation and the measurement. The slight frequency shift at f_4 for both antennas and the measured narrower bandwidth at f_3 for the ENG antenna are observed. The reason for these discrepancies is the same as that for the single-cell monopoles. Over all measured bands, the return loss is better than -10 dB. To examine the far-field characteristics, both prototypes are also measured in an anechoic chamber with co-polarized radiation patterns plotted in Figure 15. Again, the monopolar radiations are further confirmed across all corresponding bands as those measured for the single-cell monopoles.

5. CONCLUSION

In this work, novel MTM TLs which feature dual-shunt branches in the circuit model have been thoroughly investigated for the first time in the design of multifrequency monopoles. The CMTLs can be easily integrated with the planar monopoles in which the ground plane remains unaltered. For comprehensive study, the ENG and DNG, single-cell and dual-cell loaded monopoles with different configurations are designed, fabricated and measured. Numerical and experimental results both confirm that the dual ZOR modes are independent on the number of unit cells and the configurations such as ENG and DNG loading. In fact, they are determined by the shunt-branch circuit elements associated with the geometrical parameters of K-ECSSRRP. Moreover, we also find that more operating bands are obtained at the expense of some degeneration of gain, efficiency and matching when more cells are loaded. These antennas, free of any chip component and via, are readily integrated with other circuits and are compact due to the subwavelength resonance, thus they are well suited for emerging wireless communication systems such as wireless local area networks (WLAN) that require low profile, low cost, compactness, large surface area and multifunctional standard. Other geometrical parameters of K-ECSSRRP can be explored for further improvement and other shapes of CMTL elements such as CSRRs which feature one shunt branch can be employed for fewer operating bands.

ACKNOWLEDGMENT

This work was supported by the National Natural Science Foundation of China under Grant No. 60971118 and the Innovation Foundation for Postgraduate's Dissertation of Air Force Engineering University under Grant No. DY12101 and was also supported by the Foundation of Key Laboratory of Wireless Broad and Communication and Digital Signal Processing of Guangxi under Grant No. 11110. The authors want to deliver their special gratitude to the anonymous reviewers for their helpful comments.

REFERENCES

1. Liu, W. C., "Optimal design of dualband CPW-fed G-shaped monopole antenna for WLAN application," *Progress In Electromagnetics Research*, Vol. 74, 21–38, 2007.
2. Zhang, X., Y. Song, Z. H. Yan, J. B. Jiang, and Y. Y. Xia, "Design of wideband microstrip-fed plannar monopole antenna for multiband applications," *Journal of Electromagnetic Waves and Applications*, Vol. 22, Nos. 11–12, 1623–1630, 2008.
3. Cheng, P. C., C. Y. D. Sim, and C. H. Lee, "Multi-band printed internal monopole antenna for mobile handset applications," *Journal of Electromagnetic Waves and Applications*, Vol. 23, No. 13, 1733–1744, 2009.
4. Chen, W. S. and B. Y. Lee, "Novel printed monopole antenna for PDA phone and WLAN applications," *Journal of Electromagnetic Waves and Applications*, Vol. 23, Nos. 14–15, 2073–2088, 2009.
5. Anguera, J., J. P. Daniel, C. Borja, J. Mumbru, C. Puente, T. Leduc, K. Sayegrih, and P. Van Roy, "Metallized foams for antenna design: Application to fractal-shaped sierpinski-carpet monopole," *Progress In Electromagnetics Research*, Vol. 104, 239–251, 2010.
6. Panda, J. R. and R. S. Kshetrimayum, "A printed 2.4 GHz/5.8 GHz dual-band monopole antenna with a protruding stub in the ground plane for WLAN and RFID applications," *Progress In Electromagnetics Research*, Vol. 117, 425–434, 2011.
7. Jiang, Y., Y. Yu, M. Yuan, and L. Wu, "A compact printed monopole array with defected ground structure to reduce the mutual coupling," *Journal of Electromagnetic Waves and Applications*, Vol. 25, Nos. 14–15, 1963–1974, 2011.
8. Wang, B. and K.-M. Huang, "Spatial microwave power combining

with anisotropic metamaterials," *Progress In Electromagnetics Research*, Vol. 114, 195–210, 2011.

9. Chen, H., L. Huang, X. Cheng, and H. Wang, "Magnetic properties of metamaterial composed of closed rings," *Progress In Electromagnetics Research*, Vol. 115, 317–326, 2011.
10. Valagiannopoulos, C. A., "Electromagnetic scattering of the field of a metamaterial slab antenna by an arbitrarily positioned cluster of metallic cylinders," *Progress In Electromagnetics Research*, Vol. 114, 51–66, 2011.
11. Liu, L., J. Sun, X. Fu, J. Zhou, Q. Zhao, B. Fu, J. Liao, and D. Lippens, "Artificial magnetic properties of dielectric metamaterials in terms of effective circuit model," *Progress In Electromagnetics Research*, Vol. 116, 159–170, 2011.
12. Hasar, U. C. and J. J. Barroso, "Retrieval approach for determination of forward and backward wave impedances of bianisotropic metamaterials," *Progress In Electromagnetics Research*, Vol. 112, 109–124, 2011.
13. Zhou, B., H. Li, X. Zou, and T.-J. Cui, "Broadband and high-gain planar vivaldi antennas based on inhomegeneous anisotropic zero-index metamaterials," *Progress In Electromagnetics Research*, Vol. 120, 235–247, 2011.
14. Meng, F.-Y., Y.-L. Li, K. Zhang, Q. Wu, and L.-W. Li, "A detached zero index metamaterial lens for antenna gain enhancement," *Progress In Electromagnetics Research*, Vol. 132, 463–478, 2012.
15. Zari, D., H. Oraizi, and M. Soleimani, "Improved performance of circularly polarized antenna using semi-planar chiral metamaterial covers," *Progress In Electromagnetics Research*, Vol. 123, 337–354, 2012.
16. Nordin, M. A. W., M. T. Islam, and N. Misran, "Design of a compact ultrawideband metamaterial antenna based on the modified split-ring resonator and coactively loaded strips unit cell," *Progress In Electromagnetics Research*, Vol. 136, 157–173, 2013.
17. Kim, D. and M. Kim, "Narrow-beamwidth T-shaped monopole antenna fabricated from metamaterial wires," *Electronics Letters*, Vol. 44, No. 3, 180–182, Jan. 2008.
18. Antoniades, M. A. and G. V. Eleftheriades, "A folded-monopole model for electrically small NRI-TL metamaterial antennas," *IEEE Antennas and Wireless Propagation Letters*, Vol. 7, 425–428, 2008.

19. Ji, J. K., G. H. Kim, and W. M. Seong, "Bandwidth enhancement of metamaterial antennas based on composite right/left-handed transmission line," *IEEE Antennas and Wireless Propagation Letters*, Vol. 9, 36–39, 2010.
20. Ibrahim, A. A. and A. M. E. Safwat, "Microstrip-fed monopole antennas loaded with CRLH unit cells," *IEEE Transactions on Antennas and Propagation*, Vol. 60, No. 9, 4027–4036, Sep. 2012.
21. Ibrahim, A., A. M. E. Safwat, and H. El-Hennawy, "Triple-band microstrip-fed monopole antenna loaded with CRLH unit cell," *IEEE Antennas and Wireless Propagation Letters*, Vol. 10, 1547–1550, 2011.
22. Antoniades, M. A., G. V. Eleftheriades, and E. S. Rogers, "A broadband dual-mode monopole antenna using NRI-TL metamaterial loading," *IEEE Antennas and Wireless Propagation Letters*, Vol. 8, 258–261, 2009.
23. Jin, D.-L., J.-S. Hong, and H. Xiong, "Dual wideband antenna for WLAN/WiMAX and satellite system applications based on a metamaterial transmission line," *Chin. Phys. Lett.*, Vol. 29, No. 10, 104101, 2012.
24. Kokkinos, T. and A. P. Feresidis, "Low-profile folded monopoles with embedded planar metamaterial phase-shifting lines," *IEEE Transactions on Antennas and Propagation*, Vol. 57, 2997–3008, Oct. 2009.
25. Gong, J. Q., J. B. Jiang, and C. H. Liang, "Low-profile folded-monopole antenna with unbalanced composite right-/left-handed transmission line," *Electronics Letters*, Vol. 48, 813–814, Jul. 2012.
26. Zhu, J., M. A. Antoniades, and G. V. Eleftheriades, "A compact tri-band monopole antenna with single-cell metamaterial loading," *IEEE Transactions on Antennas and Propagation*, Vol. 58, No. 4, 1031–1038, Apr. 2010.
27. Palandoken, M., A. Grede, and H. Henke, "Broadband microstrip antenna with left-handed metamaterials," *IEEE Transactions on Antennas and Propagation*, Vol. 57, No. 2, 331–338, Feb. 2009.
28. Barbuto, M., F. Bilotti, and A. Toscano, "Design of a multifunctional SRR-loaded printed monopole antenna," *International Journal of RF and Microwave Computer-Aided Engineering*, Vol. 22, No. 4, 552–557, Jul. 2012.
29. Zhang, Y., W. Hong, C. Yu, Z.-Q. Kuai, Y.-D. Don, and J.-Y. Zhou, "Planar ultrawideband antennas with multiple notched bands based on etched slots on the patch and/or split ring resonators on the feed line," *IEEE Trans. Antennas Propag.*, Vol. 56, No. 9, 3063–3068, Sep. 2008.

30. Kim, J., C. S. Cho, and J. W. Lee, "5.2 GHz notched ultra-wideband antenna using slot-type SRR," *Electronics Letters*, Vol. 42, No. 6, 950–950, Aug. 2006.
31. Liu, J., S. Gong, Y. Xu, X. Zhang, C. Feng, and N. Qi, "Compact printed ultra-wideband monopole antenna with dual band-notched characteristics," *Electronics Letters*, Vol. 44, No. 12, 710–711, 2008.
32. Iizuk, H. and P. S. Hall, "Left-handed dipole antennas and their implementations," *IEEE Transactions on Antennas and Propagation*, Vol. 55, No. 5, 1246–1253, May 2007.
33. Liu, Q., P. S. Hall, and A. L. Borja, "Efficiency of electrically small dipole antennas loaded with left-handed transmission lines," *IEEE Transactions on Antennas and Propagation*, Vol. 57, No. 10, 3009–3017, Oct. 2009.
34. Azad, M. Z. and M. Ali, "Novel wideband directional dipole antenna on a mushroom like EBG structure," *IEEE Transactions on Antennas and Propagation*, Vol. 56, No. 5 1242–1250, May 2008.
35. Saenz, E., R. Gonzalo, I. Ederra, J. C. Varadaxoglou, and P. de Maagt, "Resonant meta-surface superstrate for single and multifrequency dipole antenna arrays," *IEEE Transactions on Antennas and Propagation*, Vol. 56, No. 4, 951–960, Apr. 2008.
36. Zhou, T., B.-H. Sun, Q.-Z. Liu, J.-F. Li, and Z. Xu, "Novel compact circularly polarized microstrip antenna using left-handed transmission lines," *Journal of Electromagnetic Waves and Applications*, Vol. 22, Nos. 5–6, 625–634, 2008.
37. Xu, H. X., G. M. Wang, J. G. Liang, and T. P. Li, "A compact microstrip diplexer using composite right-/left-handed transmission line with enhanced harmonic suppression," *Microwave Journal*, Vol. 54, No. 11, 112, Nov. 2011.
38. Gil, M., J. Bonache, and F. Martin, "Synthesis and applications of new left handed microstrip lines with complementary split-ring resonators etched on the signal strip," *IET Microw. Antennas Propag.*, Vol. 2, No. 4, 324–330, 2008.
39. Xu, H. X., G. M. Wang, Z. M. Xu, X. Chen, Z. W. Yu, and L. Geng, "Dual-shunt branch circuit and harmonic suppressed device application," *Applied Physics A*, Vol. 108, 497–502, Aug. 2012.
40. Sanada, A., C. Caloz, and T. Itoh, "Novel zeroth-order resonance in composite right/left handed transmission line resonators," *Proc. Asia-Pacific Microwave Conf.*, Vol. 3, 1588–1591, 2003.